Strojniški vestnik - Journal of Mechanical Engineering 69(2023)11-12, 509-521
DOI:10.5545/sv-jme.2023.680
Original Scientific Paper
Received for review: 2023-06-08
Received revised form: 2023-08-16
Accepted for publication: 2023-09-19

Active Disturbance Rejection Control Algorithm for the Driven Branch Chain of a Polishing Robot

Kaifeng Dong[1] – Jun Li[1] – Mengyao Lv[1] – Xin Li[1] – Wei Gu[2] – Gang Cheng[1,2,*]

[1] China University of Mining and Technology, School of Mechatronic Engineering, China
[2] Shangdong Zhongheng Optoelectronic Technology Co., China

To overcome poor error suppression performance and low control accuracy in the polishing robot-driven branch chain control system, this paper proposes an improved active disturbance rejection control (ADRC) from the design of the derived nonlinear function. Subsequently, the tracking differentiator (TD), extended state observer (ESO) and nonlinear state error feedback (SEF) are designed in the ADRC, and the driven branch's ADRC servo-control system is established based on the permanent magnet synchronous motor (PMSM) with each driven branch. Meantime, by establishing first-order and second-order ADRC, current-loop control, and speed-and-position-loop control are realized, respectively. Finally, this study analysed differences in the speed and motor rotor error performance between the proportional-integral-derivative (PID)control and ADRC control strategy by using Simulink. Furthermore, an experiment platform, including hardware and software, is built to validate some inclusions. The results show that the ADRC not only realises high-precision trajectory tracking control but also ensures the rapid response performance of the system.

Keywords: active disturbance rejection control, trajectory tracking, parallel mechanism, driven branch chain

Highlights

- *An ADRC algorithm-based derivable nonlinear function was established.*
- *The established first-order and second-order ADRC controller can effectively control the current loop, and speed-and-position loop, respectively.*
- *The experimental results showed that the introduction of the ADRC algorithm could achieve better performance of trajectory-tracking control during motor operation.*
- *The innovation of this paper is applying the proposed ADRC algorithm to the driven branch chain of a polishing robot.*

0 INTRODUCTION

An important element of a country's manufacturing level is the precision of optical components and ultra-precision processing technology, which is the key and foundation of advanced manufacturing technology [1]. Continued developments in the requirements of optical components' application have placed high demands on the workspace, rigidity and accuracy performance of optical polishing process equipment. The above factors mean that current ultra-precision polishing machine tools can no longer meet the relevant requirements.

The parallel mechanisms have the advantages of high rigidity, low inertia, and no accumulated machining mistakes; they have become taken over as the main structure of processing machine tools. Meanwhile, parallel robotics have grown the research of relevant scholars [2] and [3]. However, the significant nonlinearity, strong coupling, and vulnerability to external interference characteristics of the parallel robot-driven branch chain pose challenges to the controller design.

The robot trajectory was initially tracked using proportional-integral-derivative (PID) control. The PID control algorithm based on the negative feedback principle is not required to take into consideration the robot dynamics model. However, in external load disturbances, highly nonlinear and tightly coupled situations, the stability of the PID controller cannot be guaranteed, making it challenging to achieve perfect dynamic response tracking. The stability analysis of the control systems is a sensitive topic, and the Lyapunov function and the LaSalle-Youshizawa theorem were applied as commonly used methods in the book [4]. In order to deal with the above challenges, some scholars have proposed other control strategies.

The performance of the control system is enhanced by the introduction of extended state observer (ESO), which assesses all uncertain perturbations as a whole and eliminates the perturbations through feedback on the output error. In fact, many scholars have applied the ESO to a control system. As a way to transform linear results into fuzzy design processes, Precup et al. [5] proposed iterative feedback tuning (IFT) and ESO, which control servo-controllers that can be defined as integral second-order systems. Roman et al. [6] used ESO to tune proportional-integral (PI) controllers and utilized the image foresting transform (IFT) algorithm,

*Corr. Author's Address: China University of Mining and Technology, School of Mechatronic Engineering, China, chg@cumt.edu.cn

which is ultimately evaluated experimentally on a tower crane (TCS). Researchers have also studied control systems in unstable conditions. Safaei et al. [7] proposed a solution to the nonlinear subject network formation tracking problem with completely unknown dynamics and unknown perturbations. In contrast, Jin et al. [8] have enhanced the traditional controller based on PID. In order to reduce the drawbacks of bilateral control algorithms that depend on model parameters, Asad et al. [9] proposed a three-channel state convergence architecture supported by a disturbance observer.

Han and Yuan [10] summarized the idea of the cybernetics design method and formally proposed active disturbance rejection control (ADRC) including tracking differentiator (TD) [11], state error feedback (SEF) [12] and ESO [13]. Due to its features of a simple algorithm, a minimal overshoot, and great control accuracy, the ADRC is widely used in motor control [14], robot control [15], aircraft control [16], ship track control [17] and similar.

The application of ADRC in engineering practice has increased as a result of advancements in its theoretical foundation. Gao [18] used the ADRC design idea of the normalized parameter, which provided the design concept for the engineering application of ADRC. A backstep sliding mode-based attitude control law was created by Dou et al. [19], using linear ESO to estimate each system state. Roman et al. [20] proposed a virtual reference feedback tuning (VRFT) that integrates two control methods which are active immunity control and fuzzy control. The relative scholars have made plenty of theoretical progress, which lays the theoretical foundation for ADRC to be widely used. Also, the ADRC's various performances are better than PID's in some engineering applications, such as robustness, accuracy, and rapidity.

The ADRC control is a superior option to other control methods for enhancing the quality of parallel robots. Xu et al. [21] built the ESO to estimate the total disturbance, which is composed of the shipborne stable platform dynamic uncertainty, the unknown time-varying external disturbance and the coupling between the motion state variables. The Stewart platform was made by Zhang et al. [22], which is a time-varying nonlinear system for big radio telescopes. The system is fine-tuned using a disturbance rejection controller built for a single servo-branch and a control approach based on joint space. A novel 6-degree-of-freedom (6-DOF) parallel robot is driven by six novel linear motors, and Shi et al. [23] designed a fractional-order active disturbance rejection controller (FOADRC) to track their own desired trajectories for six linear motors. Based on the reduced dynamic model, Zhang et al. [24] used ADRC to track the trajectory of the Delta mechanism. A self-stable domain approach and the Lyapunov function examined the stability of the ESO and the closed-loop controller, respectively.

The above literature indicates that relevant scholars have combined ADRC control strategy with various application situations. However, the ADRC method for the driven chain of the optical mirror-polishing robot has hardly been researched. Meanwhile, the cycle of obtaining a finished mirror is usually one to two years, which is a long time for data-driven control approaches to acquire the relative data. Therefore, in order to make up for the above research gap, based on the driven chain of the optical mirror-polishing robot, the first-order and second-order ADRC controllers are established to control the current loop, and the speed-and-position loop, respectively.

The paper is organized as follows: Section 1 introduces the parallel mechanism component and control object of the optical mirror-polishing robot. Section 2 presents a servo-driven branch chain control system based on the improved ADRC algorithm. Section 3 demonstrates that the method significantly elevates the motion accuracy of the entire branch chain to reach the target position. The servo-system's motion control accuracy is guaranteed by reducing the disturbance error based on the improved ADRC controller. Section 4 concludes the paper.

1 DRIVEN CHARACTERISTIC ANALYSIS

1.1 Structure Analysis of Optical Mirror-Polishing Robot

The optical mirror-polishing robot is the study object in this paper. Its main structure consists of a rotor with 2-DOF and a parallel mechanism with 3-DOF, which is made up of a series of connections. The parallel mechanism includes UP constrained branch chain, UPS driven unconstrained branch chain, a moving platform, and a base platform distributed symmetrically. Here, U stands for Hooke joint, P stands for prismatic pair, and the constraint branch chain is connected by Hooke joint and prismatic pair. A ball hinge is used to join the moving platform to the UPS branch chain above, while a hooker hinge is used to join the opposite end of the latter to the base platform. One end of the UP-constrained branch has a fixed connection to the moving platform, while the other end is attached to the base platform by a hooker hinge that is orthogonal to the plane of the ball hinge centre point in the branch direction. The Figs. 1 and

2 display the configuration and the structure of the polishing robot.

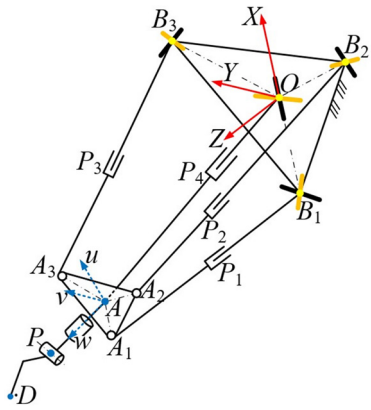

Fig. 1. *Configuration of the polishing robot*

In $B_1B_2B_3$ plane of the base platform, fixed coordinate system $O–XZY$ is established with point O as the origin. For $A_1A_2A_3$ plane of the moving platform, point A is used as origin for the construction of dynamic coordinate system $A–uvw$. In fixed coordinate system $O–XZY$, the UP branch chain axis and X axis coincide, while Z axis is perpendicular to base platform $B_1B_2B_3$ and axis can be determined by the right-hand rule. In coordinate system $A–uvw$, the u axis coincides with the UP axis, while the w axis is perpendicular to the moving platform. The v axis direction can be determined by the right-hand rule.

1.2 Driven Branch Chain Control Objects

The motor and ball-screw-based transmission system serves as the primary control object of the driven branch chain servo-system. A servo-motor from the Panasonic A6 series is fully utilized, which can create a control model based on specific parameters. The permanent magnet synchronous motor (PMSM) is a parameter and nonlinear time-varying system whose windings have an obvious saturation effect and nonlinear magnetization characteristics. To simplify the analysis, the PMSM is assumed to be an ideal motor and following assumptions are considered: the saturation of the motor core is ignored; eddy current and hysteresis loss in the motor are not accounted; the conductivity of the permanent magnet in the motor is regarded as zero; the motor rotor and permanent magnet damping have no impact; with a constant magnetic field in the air gap; the current excitation component is i_d during the directional control of pole position.

In the d-p coordinate system, the specific flux link equation is expressed as follows:

$$\begin{cases} \psi_d = L_d i_d + \psi_f \\ \psi_q = L_q i_q \end{cases}, \tag{1}$$

where ψ_d denotes the d-axis flux linkage, L_d denotes the d-axis inductance, ψ_q denotes the q-axis flux linkage, denotes the q-axis inductance, i_d denotes the straight-axis current, i_q denotes the cross-axis current.

In the d-p coordinate system, the voltage balance equation corresponding to the motor stator can be expressed as follows:

$$\begin{cases} u_d = Ri_d + \dot{\psi}_d - w_m\psi_q \\ u_q = Ri_q + \dot{\psi}_q + w_m\psi_d \end{cases}, \tag{2}$$

where u_d and u_q represent the straight-axis and cross-axis component of the stator voltage, respectively. R represents the resistance value of the stator, w_m represents the true angular velocity.

As ψ_f=0, voltage equation corresponding to the motor stator and electromagnetic torque are as follows:

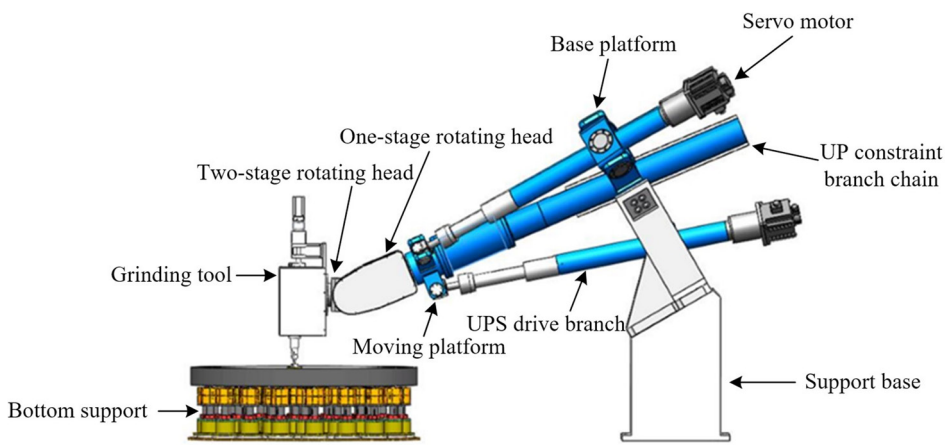

Fig. 2. *Structure diagram of the polishing robot*

$$\begin{bmatrix} u_d \\ u_q \end{bmatrix} = \begin{bmatrix} R & 0 \\ 0 & R \end{bmatrix} \begin{bmatrix} i_d \\ i_q \end{bmatrix} + \begin{bmatrix} L_d & 0 \\ 0 & L_q \end{bmatrix} \frac{d}{dt} \begin{bmatrix} i_d \\ i_q \end{bmatrix} + w_m \begin{bmatrix} -L_q i_q \\ L_d i_d + \psi_f \end{bmatrix}, \quad (3)$$

$$T_e = \frac{3}{2} p(\psi_d i_q - \psi_q i_d) = \frac{3}{2} p(\psi_f i_q + (L_d - L_q) i_d i_q). \quad (4)$$

The mechanical equation of motion is expressed as follows:

$$T = J\dot{w} + Bw + T_L, \quad (5)$$

where J represents the value of the inertia moment, T_L expresses the value of the load torque, B represents the size of the viscous damping coefficient, w states the mechanical angular velocity value corresponding to the rotor.

The control mode i_d=0 is used, so that it can achieve linear decoupling control of the electromagnetic torque, high performance of the speed regulation, and simple control scheme implementation. In terms of the direct axis current having little impact on the torque, the given value of the straight axis current is set to 0. As a result, the equation of state for the PMSM on the *d-q* axis can be determined through Eq. (6):

$$\begin{bmatrix} \dot{w} \\ \dot{i}_d \\ \dot{i}_q \end{bmatrix} = \begin{bmatrix} 0 & 1.5p\psi_f / J & -B/J \\ -R/L_d & pw & 0 \\ -pw & -R/L_q & -p\psi_f / L_q \end{bmatrix} \begin{bmatrix} i_d \\ i_q \\ w \end{bmatrix} + \begin{bmatrix} -T_L / J \\ u_d / L_d \\ u_q / L_q \end{bmatrix}. \quad (6)$$

With the performing the Laplace transform on Eq. (6), the transfer function of a PMSM is given as:

$$\frac{W(s)}{U_q(s)} = \frac{K_t}{LJs^2 + (LB + RJ)s + RB + K_t\psi_f}, \quad (7)$$

where K_t=3$p\psi_f$/2 represents the motor torque constant.

The specific model diagram can be constructed as shown in Fig. 3.

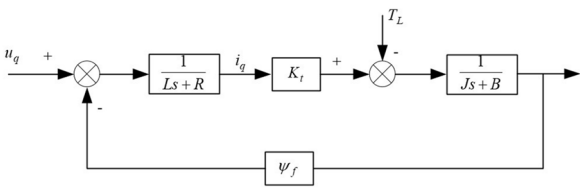

Fig. 3. *The model diagram of PMSM*

The ball screw in each driven branch converts the rotational motion of the servo-motor (see Table 1) into linear motion. Then the displacement state of each driven branch chain can be expressed as:

$$\dot{x} = \frac{r}{2\pi} w, \quad (8)$$

where r represents the ball screw lead.

Table 1. *Servo-motor parameters*

Parameter	Value
Inductance L [mH]	3.45
Resistance R [Ω]	2.6
Inertia J [kg·m²]	0.0035
Torque coefficient Kt [N·m/A]	3.58
Viscous damping coefficient B [N·s/m]	0.2
Lead screw lead r [mm]	60

2 DRIVEN BRANCH CHAIN ACTIVE DISTURBANCE REJECTION SERVO-CONTROL

2.1 The Based Derivable Nonlinear Function ADRC Controller

The TD, SEF, and ESO are three core components of ADRC, which is a control method for nonlinear and uncertain systems. About the traditional PID controller' speed and overshoot paradox, the TD tracking transition mechanism resolves the contradiction and adds the system robustness. ESO as the primary component of ADRC, which can withstand both internal and external interference while estimating the state variables of the system. The SEF control law is formed by the sum of the errors in the TD output and the ESO observation output. The controlled object input is comprised of the SEF control rule output and the ESO system interference estimator. As shown in Fig. 4, the ESO has the characteristic of real-time estimation of various disturbances in the system, so as to realize timely feedback and compensation of signal input errors, so that the whole control system has good dynamic characteristics.

The original nonlinear function is given as:

$$fal(e,\alpha,\delta) = \begin{cases} \dfrac{e}{\delta^{1-\alpha}}, |e| \le \delta \\ |e|^{\alpha}\, sign(e), |e| > \delta \end{cases}. \quad (9)$$

The derivation of Eq. (9) is:

$$fal'(e,\alpha,\delta) = \begin{cases} \dfrac{1}{\delta^{1-\alpha}}, 0 < e \le \delta \\ \alpha e^{\alpha-1}, e > \delta \end{cases}. \quad (10)$$

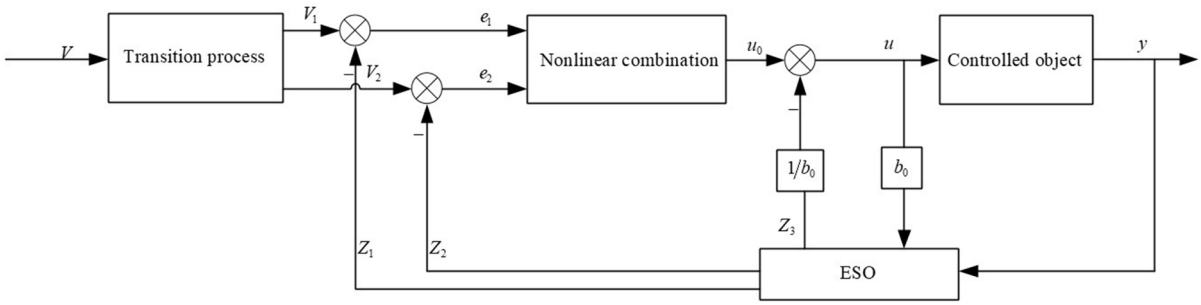

Fig. 4. *ADRC control block diagram*

From the mathematic perspective, the function *fal* can be observed to be continuous. For a kind of piecewise function, its switching point cannot be derived. Also, the slope of the function *fal* in the linear segment has an inverse relationship with the size of the function *fal*'s linear interval 2δ. Under this premise, the driven branch chain's performance under the ADRC will eventually become unstable when the linear interval 2δ is minimal. This is because the dynamic gain of the function *fal* will abruptly change, leading to a high-frequency chattering phenomenon. To lessen system tremor and increase stability, the function *fal* needs to be enhanced when the linear interval is minimal.

According to the characteristics of the function *fal*, its expression is optimized accordingly. Based on ensuring the continuity of the function image, it is required to be derivable at the switching point of the segmented function, and the optimized expression of the function *newfal* is as follows:

$$newfal = \begin{cases} k_1 \sin(e) + k_2 \tan(e), |e| \le \delta \\ |e|^{\alpha} \, sign(e), |e| > \delta \end{cases}, \quad (11)$$

where k_1 and k_2 can be determined by the following equation:

$$\begin{cases} k_1 = \dfrac{\delta^{\alpha} - \alpha\delta^{\alpha-1}\sin(\delta)\cos(\delta)}{\sin^3(\delta)} \\ k_2 = \dfrac{\alpha\delta^{\alpha-1}\sin(\delta) - \delta^{\alpha}\cos(\delta)}{\sin(\delta)\tan^2(\delta)} \end{cases}. \quad (12)$$

From the design concept of the function *newfal*, it can be known that it is conductible at the switching point, and the derivative value does not change abruptly at the $e = \pm\delta$, which ensures the stability of the driven chain motion under the active disturbance rejection controller. Therefore, by optimizing the *fal* in the active disturbance rejection controller to the function *newfal*, the stability of the system will be guaranteed.

2.2 Current Loop Control Based on First-order Active Disturbance Rejection Controller

To achieve motor speed, position, and torque control, electromagnetic torque control, which essentially controls the three-phase alternating current (AC) and direct current (DC) in the model, is especially important. In an AC PMSM servo-control system, the control of the inner ring current loop is a prerequisite for achieving high-performance servo-control. Therefore, the current loop control should make its steady-state characteristics have relatively high quality, and the transient response ought to be fairly quick. PI regulators are now commonly used. However, if the controller current loop has parameter changes, a dead zone effect, or back electromagnetic fields (EMF), controller disturbance suppression and command tracking capabilities will not meet the relevant requirements. In order to cope with the above-mentioned undesirable factors, the paper proposes an improved first-order ADRC.

The current loop dynamic equation for the *q*-axis is:

$$i_q = \frac{u_q^*}{L_q} - \left(\frac{R}{L_q} i_q + \frac{w_m}{L_q} \psi_f \right) - \frac{u_q^* - u_q + w_m L_d i_d}{L_d}. \quad (13)$$

The control amount is set as $u = u_q$. Due to the influence of temperature, magnetic field, vibration, and external working conditions on the inductor, the known disturbance is $f(x) = -Ri_q / L_q - w_m\psi_f / L_q$, and $f(x)$ can be calculated by the motor parameters and the shaft feedback current. Also, the unknown disturbance is set as , and the total disturbance of the system is $w(t) = -\bar{u}_q^* - u_q + w_m L_d i_d / L_q$.

Thus, the equation of the *q*-axis current state is as follows:

$$\begin{cases} y = x_1 = i_q \\ \dot{x}_1 = x_2 + bu. \\ x_2 = a(t) \end{cases} \tag{14}$$

To ensure the steady of inner current loop, the equation of state is a first-order link, and the ADRC controller can be ensured as follows:

(1) The TD is:

$$\begin{cases} e_{11} = v_{11} - i_q^* \\ \dot{v}_{11} = v_{12} \\ \dot{v}_{12} = fhan(e_{11}, v_{12}, r_0, h) \end{cases}, \tag{15}$$

where i_q^* is a given current signal, v_{12} is the differential signal of q-axis current reference value.

(2) The ESO is:

$$\begin{cases} e_{12} = z_{11} - x_1 \\ \dot{z}_{11} = z_{12} - \beta_{11} fal(e_{12}, \alpha_{11}, \delta_1) + bu, \\ \dot{z}_{12} = -\beta_{12} fal(e_{12}, \alpha_{12}, \delta_1) \end{cases} \tag{16}$$

where $x_1 = i_q$ is the system output, z_{11} is the x_1 tracking value, z_{12} is the observation of the current loop system total disturbance.

(3) The NLSEF control law is:

$$\begin{cases} e_{13} = v_{12} - z_{11} \\ u_0 = -\beta_{13} e_{13} \\ u = u_0 - z_{12} / b \end{cases}, \tag{17}$$

where $b = 1/L_q$ states current loop compensation coefficient; $u = u_q^*$ represents the reference value for q-axis voltage.

The reference current i_q^* on q-axis passes through first-order tracking differentiator, then the corresponding differential signal will be obtained. Also, i_q goes through expanding state observer to obtain total perturbation of the system and the corresponding tracking signal. Meanwhile, the proportional adjustment is implemented, and the appropriate feed-forward compensation is given leading to the reference input u_q being obtained.

2.3 Position Speed Control Based on Second-order Active Disturbance Rejection Controller

To reduce the adverse effects of coupling between torque current and exciting current, various external disturbances and internal parameter perturbations on the servo-control system. The position-based output equation second-order ADRC is proposed in the paper. One controller handles both rotational speed and position. The revolution speed of PMSM is:

$$\frac{d^2\theta}{dt^2} = \frac{d\omega}{dt} = \frac{3p\psi_f}{2J} i_q - \frac{T_L}{J} - \frac{B\omega}{J}, \tag{18}$$

$$\ddot{\omega} = -B\dot{\omega} - \frac{p\psi_f^2}{JL}\omega - \frac{3p\psi_f R}{2JL} i_q - \frac{3p^2\psi_f^2}{2JL}\omega - \frac{p}{J}\dot{T}_L + \frac{3p\psi_f u_q}{2JL}. \tag{19}$$

The control variable is $u_0 = i_q$, a comprehensive disturbance is $f(x_1, x_2) = -Bw/J$, load torque disturbance and external uncertain disturbance are $w(t) = -rT_L/2\pi J$ and $b = 3rp\psi_f/4\pi J$, respectively.

Therefore, there is $\ddot{\theta} = a(t) + bu_0$, where $a(t) = f(x_1, x_2) + w(t)$.

Then the equation of state can be rewritten as:

$$\begin{cases} y = x_1 = \theta \\ \dot{x}_1 = x_2 = \omega = \dfrac{d\theta}{dt} \\ \dot{x}_2 = \dot{\omega} = \hat{a}(t) + b_0 u_0 \end{cases}, \tag{20}$$

where $\hat{a}(t)$ represents an estimation of the total perturbation, b_0 represents an estimation of the b.

Based the principle of ADRC, the corresponding TD, ESO, and NLSEF are designed, as follows:

(1) The TD is:

$$\begin{cases} e_{21} = v_{21} - \theta* \\ \dot{v}_{21} = v_{22} \\ \dot{v}_{22} = fhan(e_{21}, v_{22}, r_0, h) \end{cases}, \tag{21}$$

where θ^* states specific position of the given rotor, v_{21} represents the tracking signal corresponding to θ^*, v_{22} is the θ^* corresponding differential signal.

(2) The ESO is:

$$\begin{cases} e_{22} = z_{21} - \theta \\ \dot{z}_{21} = z_{22} - \beta_{21} e_{22} \\ \dot{z}_{22} = z_{23} - \beta_{22} fal(e_{22}, \alpha_{21}, \delta_2) + b_0 i_q^*, \\ \dot{z}_{23} = -\beta_{23} fal(e_{22}, \alpha_{22}, \delta_2) \end{cases} \tag{22}$$

where θ represents specific feedback signal corresponding to the rotor position, z_1 expresses estimated tracking value corresponding to the actual position θ, z_2 represents differential signal corresponding to z_1, z_3 is total perturbation observation, e_{02} represents error value of the z_1 tracking output value θ, i_q^* expresses given value of the q-axis current command.

(3) The NLSEF control law is:

$$\begin{cases} e_{23} = v_{21} - z_{21} \\ e_{24} = v_{22} - z_{22} \\ u_0 = \beta_1 fal\left(e_{23}, \alpha_{23}, \delta_2\right) + \beta_2 fal\left(e_{24}, \alpha_{24}, \delta_2\right). \\ i_q^* = u_0 - \dfrac{z_3}{b_0} \end{cases} \quad (23)$$

After θ^* passing the TD, the tracking signal and the corresponding differential signal will be obtained. And after θ going through the ESO, total disturbance estimation and system state estimation will be obtained. After the error nonlinear adjustment, the corresponding reference signal i_q^* is gained in feedforward compensation process. Thus, high-precision position control is achieved in the ADRC controller.

The currently under-study servo-control system encompasses three close-loop, which is the position-loop, current-loop and velocity-loop. The velocity-loop controller in the central loop is used to realize the stable adjustment of velocity. The position-loop controller in the outer loop is used to compare actual feedback position and rotor position-related instructions under the given command, and makes the error signal perform certain calculations by position-loop controller.

Subsequently, the speed reference signal could be obtained by the position-loop. Comparing the speed reference signal with rotor feedback signal to obtain the corresponding error, then control the error to get the relative current control volume of current loop. The current-loop controller in the inner loop is used to obtain the corresponding reference voltage as well as signalled the inverter circuit. The servo-system will produce a three-phase sinusoidal current which is fed into the motor, and destination of motor servo-control is accomplished.

3 SIMULATION RESULTS AND EXPERIMENT

3.1 Experimental Verification

In this paper, an experimental platform of the optical mirror-polishing robot is established to test the performance of the ADRC algorithm in motion trajectory tracking. When the robot is polishing optical mirrors, once the entire optical mirror polishing process and polishing paths are determined, the fast, stable and high-precision point-to-point motion of the polishing robot executing mechanism can be achieved. The hardware component of the experimental control system mainly includes one industrial personal computer (IPC), one programmable multi-axes controller (PMAC), some ball screws, one servo-system and various sensors. A detection module and a data processing component are part of the software system, and they are both electrically coupled to the power module. The data processing module's input electrical connection human-machine interaction module and detection module, as well as its output electrical connection motion control module. The detection module can measure the electrical signal in the power module, and the power module can accept and carry out the power cut-off command given by

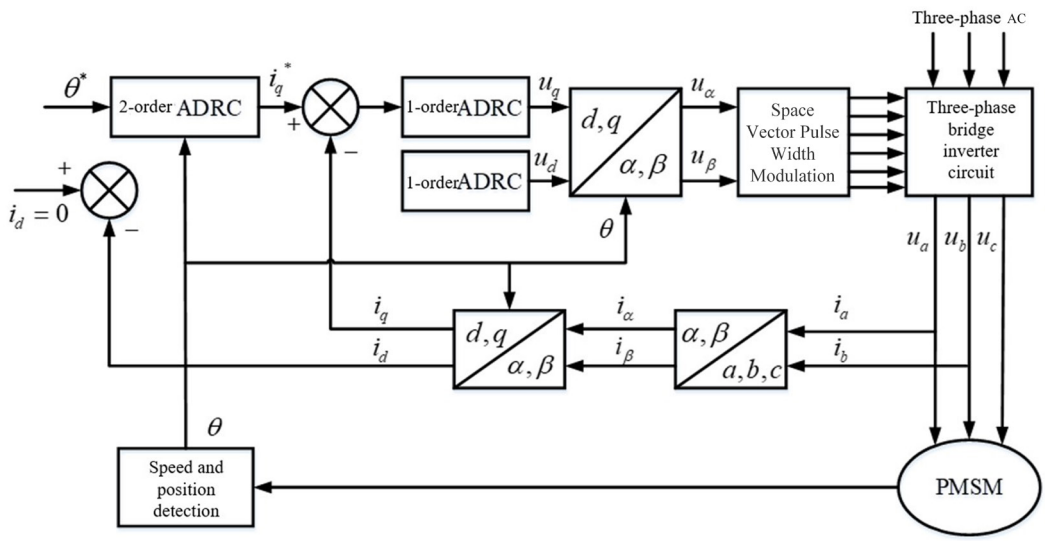

Fig. 5. *Permanent magnet synchronous motor active disturbance rejection servo-control diagram*

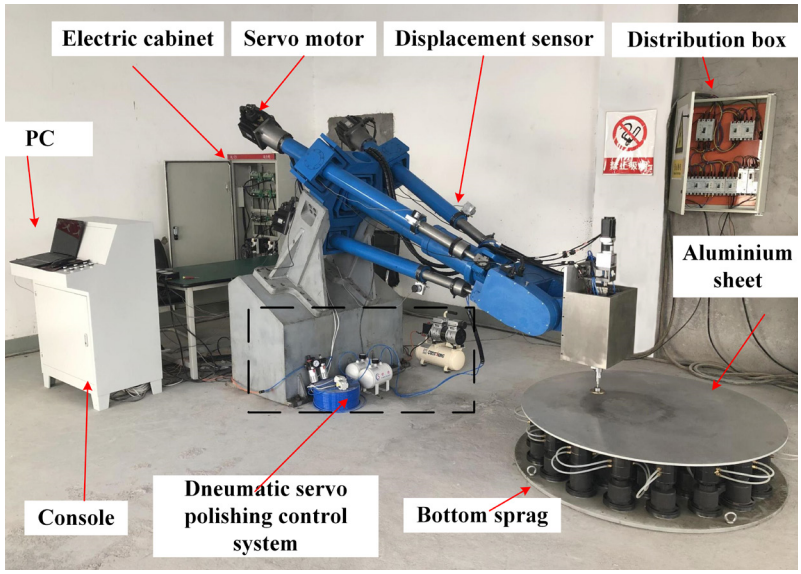

Fig. 6. *Experimental body and experimental environment*

the data processing module. The processing device is electrically coupled to both the input and output ends of the motion control and detection modules.

In order to verify that the input motion instructions can achieve the predetermined motion of the robot, this paper conducts real-time measurements of the displacement of each branch chain and the trajectory tracking of the centre point of the moving platform. Only a simple trajectory motion curve is given here. Fig. 6 show experimental body and experimental environment.

The motion trajectory of the centre point of the moving platform is input into the designed software platform, which solves through the inverse kinematics and controls each driven branch chain to follow the given trajectory. The trajectory of the centre point of the given moving platform is an arc curve as the trajectory tracking accuracy experiment test path. In order to reflect the control performance of the designed controller better, the manipulator is controlled by writing in the multi-axis motion controller written in the PID and ADRC control algorithms. And the encoder and displacement sensor inside the motor has been used to collect relevant data. The individual-driven chain displacement tracking error is the result of the data fitting diagrams at Figs. 7 to 9.

According to the displacement change data information of the three driven branch chains, the paper performs kinematics calculations to obtain the trajectory tracking situation of the moving platform centre point under the application of the PID and ADRC control algorithms. Also, the tracking error of

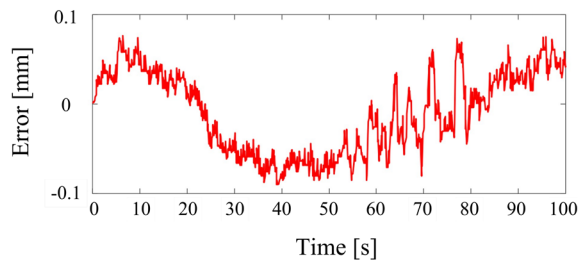

Fig. 7. *Displacement tracking error of the first driven branch*

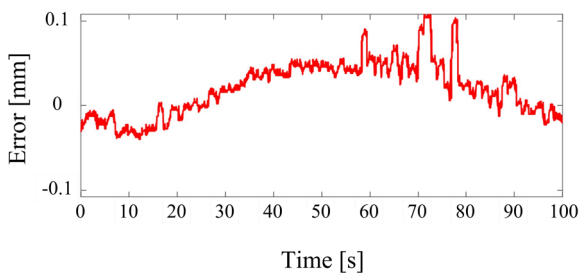

Fig. 8. *Displacement tracking error of the second driven branch*

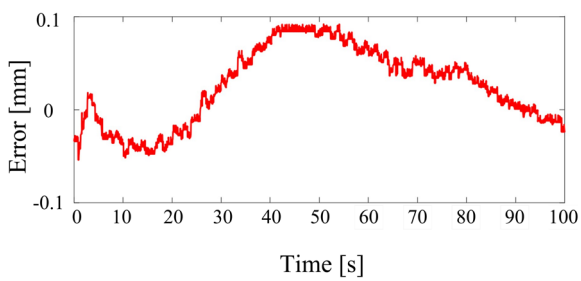

Fig. 9. *Displacement tracking error of the third driven branch*

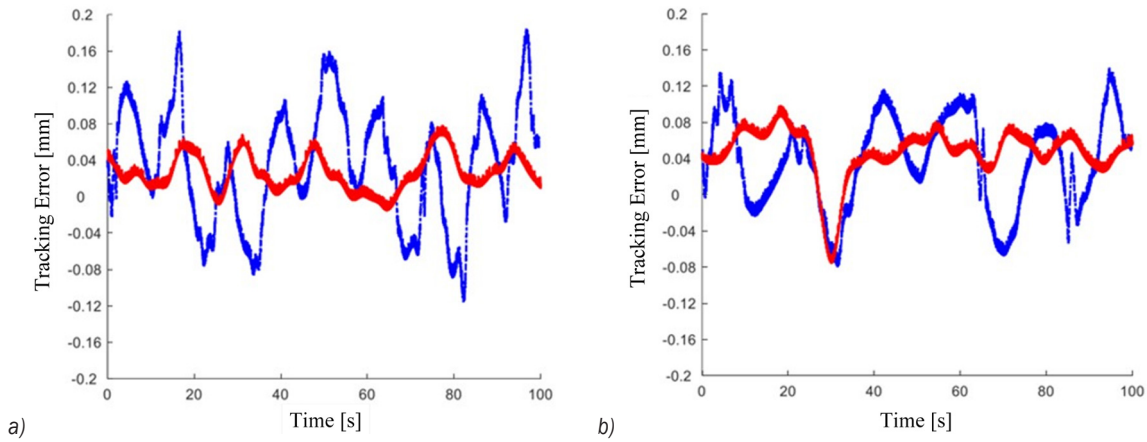

Fig. 10. *Trajectory tracking error at the centre point of the moving platform; a) X-direction; b) Y-direction*

the mobile platform is listed in Table 2 to analyse the operating accuracy of the moving platform based on PID and ADRC.

In Fig. 10, the red data curve is the control effect curve created in this article based on ADRC, whereas the blue data curve represents the PID control effect curve. Only the data results in the *X* and *Y* directions of the centre point of the moving platform are assessed. As shown in Table 2, the PID control algorithm has an error range of around 0.3 mm, but the algorithm under study in the research has an error range of approximately 0.1 mm. The ADRC overall control effect outperforms the PID algorithm by a wide margin.

Table 2. *Trajectory tracking error of the mobile platform*

	Max. in X	Amplify in X	Max. in Y	Amplify in Y
ADRC	0.08	0.1	0.09	0.14
PID	0.18	0.3	0.17	0.22

3.2 Driven Branch Chain Response Verification Experiment

The control object of the driven branch servo-system primarily focused on the transmission system what is composed of the motor and ball screw to verify the stability and control accuracy of the established ADRC control algorithm. In this paper, first-order active disturbance rejection controller of the current

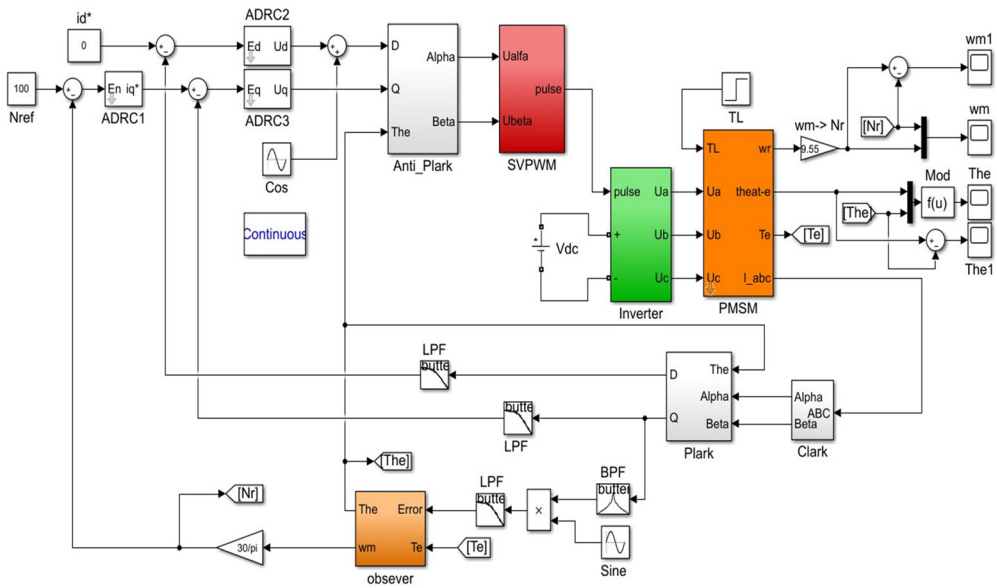

Fig. 11. *Simulink model diagram of permanent magnet synchronous motor*

loop and second-order active disturbance rejection controller of position speed loop are established. The Simulink model diagram of the PMSM is constructed as shown in Fig. 11. Subsequently, the motor rotation estimation error of the ADRC system and the speed response under the two control strategies are measured, respectively. At the same time, relevant characteristics are analysed, and corresponding conclusions are drawn.

In this paper, the variability of parameters such as electromagnetic torque, *d*-axis current, and *q*-axis current of the motor is gained by inputting varying external load torque to the system. As shown in Figs. 12 and 13, in addition to the peak phenomenon of the motor performance indicators during the start-up phase, the electromagnetic torque fluctuates at t = 0.05 s, which is from –4 N·m is changed to 0 N·m, and it can be assumed that a sudden change in the load torque occurs. The *d*-axis current and *q*-axis current fluctuate when the load torque varies abruptly, but they quickly return to a stable value since the ADRC can swiftly suppress the perturbations when the load torque fluctuates.

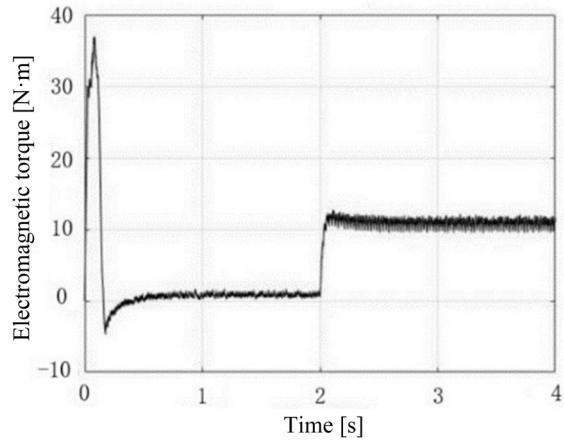

Fig. 12. *Electromagnetic torque response diagram*

In order to test the capacity of the ADRC control system to resistant to load disturbances, the system is

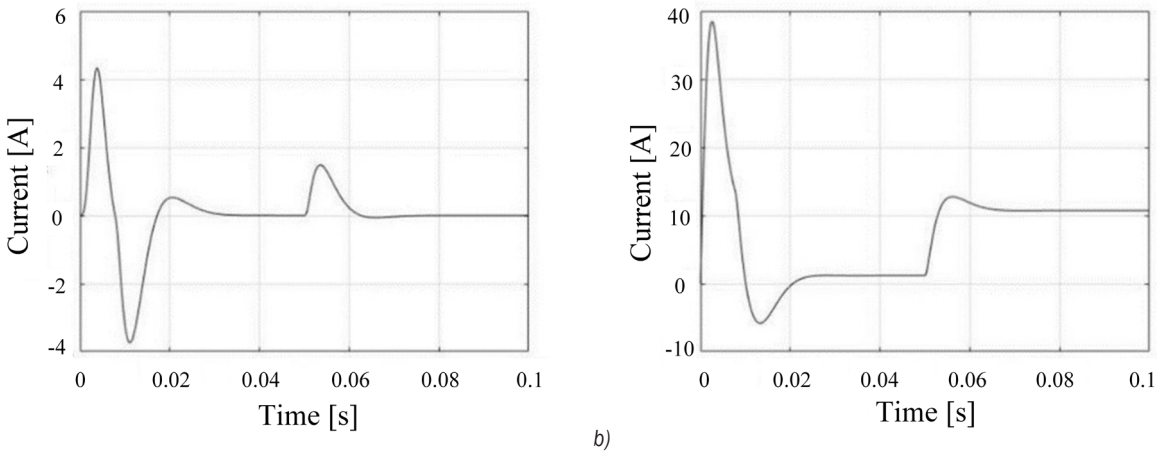

a) *b)*

Fig. 13. *Current response diagram a) d-axis; b) q-axis*

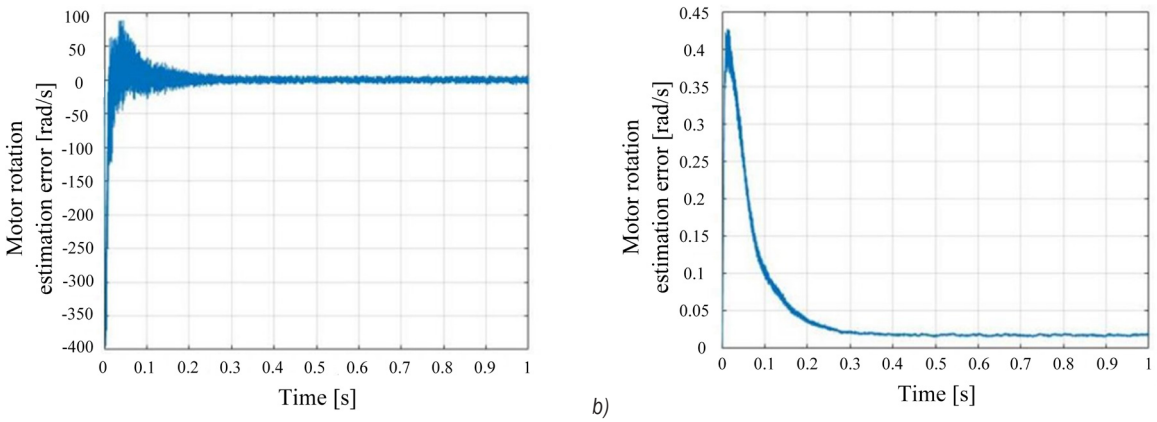

a) *b)*

Fig. 14. *Motor rotation estimation error; a) motor speed; b) motor position*

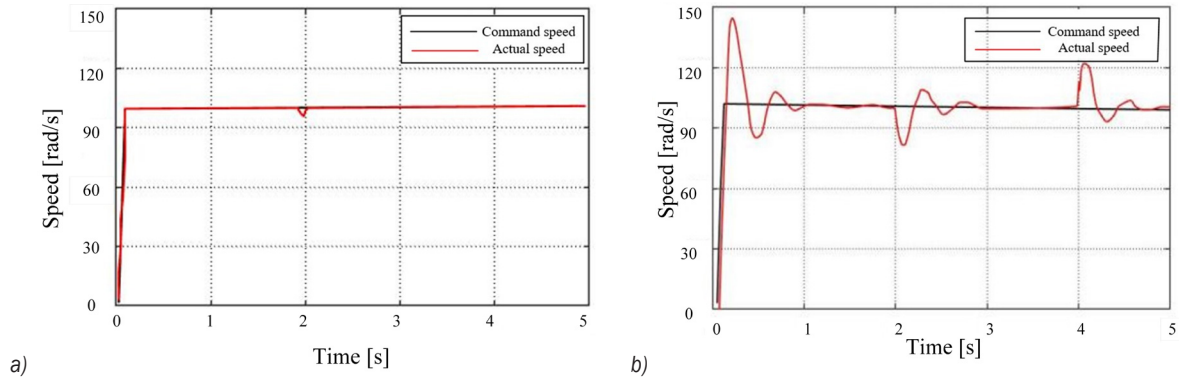

Fig. 15. *Speed response and load disturbance curve; a) ADRC regulation, b) PID regulation*

configured to a stated speed of 100 r/min and an initial load torque of 30 N·m. Fig. 14 shows the variation curves of the servo-motor speed estimation error and rotor position estimation error of the system under the ADRC. As seen in Fig. 14, the motor's rotor position error and rotational speed error are initially not very stable, especially the rotational speed error, which exhibits some fluctuation phenomena. However, with the aid of the ADRC's adjustment, the information for errors gradually tends to zero in a short time, and the fluctuation range is narrowing from 0 s to 0.3 s.

To test the speed response of the system with ADRC and PID controllers when a load is applied, in this study, Simulink experiments are performed to obtain the trajectory tracking of the speed response under the two control methods. The system is provided a step signal with output final value of 100 r/min. The simulation time is 5 s, in order to test the ability of ADRC and PID controllers to resist disturbances, a load torque of 10 N·m is applied at t = 2 s in this experiment, and the simulation results are shown in Fig. 15.

As shown in Table 3, after the motor starts to run, the speed reaches the set value of about 1 s. At the same time, overshooting of the speed occurs, the maximum speed is about 145 r/min, and the overshooting amount is 45 %. At t = 2 s, the motor speed fluctuation at a pace of around 1 s to temporarily restore stability, but the motor speed fluctuation oscillates again in 4 s to 5 s. In Fig. 15a, the motor starts to run and reaches the set value almost at the same time as the commanded speed, which is about 1s earlier than the traditional PID control. This improves the tracking performance of the system and eliminates overshooting amounts. Also, when the 10 N·m load is applied to the system at t = 2 s, the system undergoes a slight fluctuation, but the rotational speed returns to stability within about 0.1 s, which is 0.9 s less than that of the conventional PID.

Table 3. *Speed response and load perturbation*

	Given rate [rad/s]	Load [N·m]	Overshoot [%]	Disturbance value [rad/s]	Rise time [s]	Max. speed [rad/s]
ADRC	100	10	0	2.5	0.1	100
PID	100	10	45	17	1	145

From the comparison of the aforementioned simulation results, it is clear that the ADRC-based synchronous control of the motor is less affected by the extrinsic load torque. Meanwhile. the motor can track up to the target speed quickly, and the robustness is also improved when compared to the traditional PID control strategy.

4 CONCLUSIONS

To meet the demand for parallel robot control in the process of processing optical mirrors, a new type of ADRC is established based on derivable function, and the improved ADRC algorithm is embedded in the driven branch chain servo-system of the polishing robot. A first-order active disturbance rejection controller for the current loop control and second-order active disturbance rejection controller for speed-and-position loop control are designed. The control model is created by using Simulink; a specific experimental platform and corresponding experimental environment are built to verify the performance of the ADRC algorithm on the trajectory tracking of robot motion. It is validated that the introduction of active disturbance rejection algorithm can effectively suppress error information, improve accuracy and efficiency in the motor operation process. When facing load disturbance, the speed

response shows that the ADRC can more effectively ensure the operation state of the servo-system than PID control, and stability of the position and attitude adjustment process of each driven branch chain are guaranteed. To some extent, it can explain the high accuracy control of the established ADRC algorithm. Moreover, idealized elements like swirl and hysteresis loss, the conductivity of a permanent magnet and permanent magnet damping have little impact on the outcomes of the experiment.

5 ACKNOWLEDGEMENTS

This work was supported by the Priority Academic Program Development of Jiangsu Higher Education Institutions (PAPD) and the National Natural Science Foundation of China (Grant No. 52275039) and is gratefully acknowledged. The authors also would like to thank the Shandong Zhongheng Optoelectronic Technology Co., Ltd. for providing experimental devices and physical prototype of the hybrid robot for verifying effectiveness of the proposed approach.

6 REFERENCES

[1] Wang, D.S., Da, S., Liu, W.G. (2010). Ultra-precision optical component manufacturing technology. *Defense Manufacturing Technology*, no. 5, p. 5-10.

[2] Rasheed, T., Long, P., Caro, S. (2020). Wrench-feasible workspace of mobile cable-driven parallel robots. *ASME Journal of Mechanisms and Robotics*, vol. 12, no. 3, art. ID 031009, **DOI:10.1115/1.4045423**.

[3] Cheng, G., Gu, W, Yu, J.L., Tang, P. (2010). Overall structure calibration of 3-UCR parallel manipulator based on quaternion method. *Strojniški vestnik - Journal of Mechanical Engineering*, vol. 57, no. 10, p. 719-729, **DOI:10.5545/sv-jme.2010.167**.

[4] Precup, R.E., Roman, R.C., Safaei, A. (2022). Introduction. *Data-Driven Model-Free Controllers*. CRC Press, Boca Raton, p. 1-22, **DOI:10.1201/9781003143444-1**.

[5] Precup, R.E., Preitl, S., Rudas, I.J., Tomescu, M.L., Tar, J.K. (2008). Design and experiments for a class of fuzzy controlled servo systems. *IEEE/ASME Transactions on Mechatronics*, vol. 13, no, 1, p. 0-35, **DOI:10.1109/tmech.2008.915816**.

[6] Roman, R.C., Precup, R.E., Hedrea, E.L., Preitl, S., Zamfirache, I.A., Bojan-Dragos, C.A., Petriu, E.M. (2022). Iterative feedback tuning algorithm for tower crane systems. *Procedia Computer Science*, vol. 199, p. 157-165, **DOI:10.1016/j.procs.2022.01.020**.

[7] Safaei, A., Mahyuddin, M.N. (2018). A solution for the cooperative formation-tracking problem in a network of completely unknown nonlinear dynamic systems without relative position information. *International Journal of Systems Science*, vol. 49, no, 16, p. 3459-3475, **DOI:1080/00207721.20198.15442755**.

[8] Jin, Z.J., Cheng, G., Xu, S.C., Yuan, D.P. (2022). Error prediction for a large optical mirror processing robot based on deep learning. *Strojniški vestnik - Journal of Mechanical Engineering*, vol. 68, no. 3, p. 175-184, **DOI:10.5545/sv-jme.2021.7455**.

[9] Asad, M.U., Farooq, U., Gu, J., Liu, R., Abbas, G., Balas, V. (2021). Disturbance-observer-supported three-channel state convergence architecture for bilateral teleoperation systems. *ACTA Press*, vol. 36, no. 5, p. 316-324, **DOI:10.2316/J.2021.206-0411**.

[10] Han, J.Q., Yuan, L.L. (1999). The discrete form of tracking - differentiator. *Journal of Systems Science and Mathematical Sciences*, vol. 19, no. 3, p. 268-273.

[11] Wang, C.W., Ji, X.H., Zhang, Z.Y., Zhao, B., Quan, L., Plummer, A.R. (2022). Tracking differentiator-based back-stepping control for valve-controlled hydraulic actuator system. *ISA Transactions*, vol. 199, p. 208-220, **DOI:10.1016/j.isatra.2021.02.028**.

[12] Chen, Q., Shi, H.H., Sun, M.X. (2020). Echo state network-based backstepping adaptive iterative learning control for strict-feedback systems: An error-tracking approach. *IEEE Transactions on Cybernetics*, vol. 50, no. 7, p. 3009-3022, **DOI:10.1109/TCYB.2019.2931877**.

[13] Sancak, K.V., Bayraktaroglu, Z.Y. (2021). Bayraktaroglu Observer-based friction compensation in heavy-duty parallel robot control. *Journal of Mechanical Science and Technology*, vol. 35, p. 3693-3704, **DOI:10.1007/s12206-021-0738-2**.

[14] Tang, X.G., Yang, G.Y., Xun, H. (2022). Permanent magnet synchronous motor RBF network magnetic field vector control system for robotic arms. *Journal of Beijing Institute of Technology*, vol. 42, no. 10, p. 1089-1096, **DOI:10.15918/j.tbit1001-0645.2021.267**. (in Chinese)

[15] Yang, L.B., Zhang, W.G., Huang, D.G. (2015). Robust trajectory tracking of quadcopter based on attitude decoupling of ADRC. *Transactions of Beijing University of Aeronautics & Astronautics*, vol. 41, no. 6, p. 1026-1033, **DOI:10.13700/j.bh.1001-5965. 2014.0392**. (in Chinese)

[16] Meng, Z.P., Yang, L.Q., Wang, B., Liu, Y.B. (2022). ADRC controller design for folding wing vehicle based on improved equilibrium optimization. *Journal of Beijing University of Aeronautics & Astronautics*, **DOI:10.13700/j.bh.1001-5965.2022.0698**. (in Chinese)

[17] Li, R.H., Li, T.S., Piao, R.X. (2013). Under-driven surface vessel track tracking self-disturbance rejection control. *Journal of Dalian Maritime University*, vol. 39, no. 2, p. 5-8, **DOI:10.16411/j.cnki.issn1006-7736.2013.02.005**. (in Chinese)

[18] Gao, Z.Q. (2013). On the foundation of active disturbance rejection control. *Control Theory and Technology*, vol. 30, no. 12, p. 1498-1510, **DOI:10.7641/CTA.2013.31087**.

[19] Dou, J.X., Kong, X.X., Wen, B.C. (2016). Reverse sliding mode self-disturbance rejection control and stability of quadcopter attitude. *Journal of Northeastern University (Natural Science Edition)*, vol. 37, no. 10, p. 1415-1420, **DOI:10.3969/j.issn.1005.3026.2016.10.011**. (in Chinese)

[20] Roman, R.C., Precup, R.E., Petriu, E.M. (2021). Hybrid data-driven fuzzy active disturbance rejection control for tower crane systems. *European Journal of Control*, vol. 58, p. 373-387, **DOI:10.1016/j.ejcon.2020.08.001**.

[21] Xu, M., Du, J.L., He, G.J. (2020). Mailah stability control law design of parallel three-degree-of-freedom shipborne

stable platform based on ADRC. *Journal of Dalian Maritime University*, vol. 46, no. 1, p. 20-28, **DOI:10.16411/j.cnki.issn1006-7736.2020.01.003**. (in Chinese)

[22] Zhang, Y.F., Zhang, A., Duan, B.Y. (2005). Disturbance rejection control and experimental study of fine-tuning system of large radio telescope. *Mechanical Strength*, no. 6, p. 748-751, **DOI:10.16579/j.issn.1001.9669.2005.06.007**. (in Chinese)

[23] Shi, X.X., Huang, J.C., Gao, F.Z. (2020). Fractional-order active disturbance rejection controller for motion control of a novel 6-DOF parallel robot. *Mathematical Problems in Engineering*, vol. 2020, art. ID 3657848, **DOI:10.1155/2020/3657848**.

[24] Zhang, Y., Chen, Z.Q., Zhang, X.H., Sun, Q.L., Sun, M.W. (2018). A novel control scheme for quadrotor UAV based upon active disturbance rejection control. *Aerospace Science & Technology*, vol. 79, p. 601-609, **DOI:10.1016/j.ast.2018.06017**.